PROCEEDINGS OF SPIE

SPIEDigitalLibrary.org/conference-proceedings-of-spie

Broadband PureGaB Ge-on-Si photodiodes responsive in the ultraviolet to near-infrared range

Knežević, Tihomir, Krakers, Max, Nanver, Lis

Tihomir Knežević, Max Krakers, Lis K. Nanver, "Broadband PureGaB Ge-on-Si photodiodes responsive in the ultraviolet to near-infrared range," Proc. SPIE 11276, Optical Components and Materials XVII, 112760I (3 March 2020); doi: 10.1117/12.2546734

SPIE.

Event: SPIE OPTO, 2020, San Francisco, California, United States

Broadband PureGaB Ge-on-Si photodiodes responsive in the ultraviolet to near-infrared range

Tihomir Knežević*[a, b], Max Krakers[b], Lis K. Nanver[b]
[a]University of Zagreb, Faculty of Electrical Engineering and Computing, Micro and Nano Electronics Laboratory, Croatia; [b]University of Twente, Faculty of Electrical Engineering Mathematics & Computer Science, Enschede, The Netherlands

ABSTRACT

Optical characterization of PureGaB germanium-on-silicon (Ge-on-Si) photodiodes was performed for wavelengths between 255 nm and 1550 nm. In PureGaB technology, chemical vapor deposition is used to grow germanium islands in oxide windows to the silicon substrate and then cap them *in-situ* with nm-thin layers of first gallium and then boron, thus forming nm-shallow p^+n diodes. These PureGaB Ge-on-Si photodiodes are CMOS compatible and characterized by low leakage currents. Here they are shown to have high responsivity in the whole ultraviolet (UV) to near infrared (NIR) wavelength range. Particularly, two sets of diodes were studied with respect to possible detrimental effects of the Al metallization/alloying process steps on the responsivity. Al-mediated transport of the Ge and underlying Si was observed if the PureGaB layer, which forms a barrier to metal layers, did not cover all surfaces of the Ge islands. A simulation study was performed confirming that the presence of acceptor traps at the Ge/Si interface could decrease the otherwise high theoretically attainable responsivity of PureGaB Ge-on-Si photodiodes in the whole UV to NIR range. A modification of the device structure is proposed where the PureGaB layer covers not only the top surface of the Ge-islands, but also the sidewalls. It was found that to mitigate premature breakdown, it would be necessary to add p-doped guard rings in Si around the perimeter of Ge islands, but this PureGaB-all-around structure would not compromise the optical performance.

Keywords: broadband photodiode, ultraviolet photodiode, near-infrared photodiode, Ge-on-Si, Ge diodes, pure gallium and pure boron (PureGaB), responsivity, light emission measurements, simulations

1. INTRODUCTION

Detection of wavelengths from the ultraviolet (UV) to near-infrared (NIR) range (200-1550 nm) coupled with CMOS compatibility holds a promise of increasing functionality in a variety of optoelectronic systems. Some applications, i.e. optical communication[1], medical imaging[2] and light detection and ranging (LIDAR)[3], strive to develop high sensitivity detectors for a specific narrow band of wavelengths. Other fields such as spectroscopy[4], military[5] and security[6] applications profit from having a single broadband sensor to cover detection of photons in the whole UV to NIR range. In semiconductor technology, broadband detection can be achieved by using appropriate materials and/or utilizing various physical effects to make the optoelectronic devices[7–12]. However, only the integration of broadband sensors with CMOS circuitry would deliver the aspired boost in functionality. This has, for example, led to work on the monolithic integration of graphene in CMOS as a phototransistor that forms the basic component of broadband image sensors[13]. Nevertheless, seamless integration of materials such as graphene in CMOS is still technologically challenging[14]. Germanium can also be used as a semiconductor material for making detectors that are responsive up to NIR wavelengths, with the advantage that Ge can be easily grown directly on silicon and monolithically integrated in CMOS. In several Ge-on-Si technologies, the fabrication of high performance photodetectors has been demonstrated[15–17].

A comparison of the optical constants and internal quantum yields of Si and Ge[18–20] indicates that Ge photodiodes could even outperform Si diodes for detection of UV light if the pn-junction in Ge is brought close enough to the surface. There are several methods used for forming shallow pn-junctions in Ge devices such as ion implantation[21], monolayer doping[22] or spin-on-dopants activated by laser annealing[23,24]. Defect-free pn junctions are also grown epitaxially by chemical vapor deposition (CVD) in blanket depositions, requiring mesa etching for device isolation[25]. In contrast, in PureGaB technology, chemical vapor deposition is used to grow germanium islands in oxide windows to the silicon substrate and then cap them *in-situ* with nm-thin layers of first gallium and then boron, thus forming nm-shallow p^+n diodes. PureGaB Ge-on-Si photodiodes are CMOS compatible and characterized by low leakage currents. The deposition of pure B to form p^+-like regions is already used in commercial Si photodiodes. These "PureB" Si photodiodes have nm-shallow junctions with

*tihomir.knezevic@fer.hr; phone +385 1 6129-564; minel.fer.hr

Optical Components and Materials XVII, edited by Shibin Jiang, Michel J. F. Digonnet,
Proc. of SPIE Vol. 11276, 112760I · © 2020 SPIE · CCC code: 0277-786X/20/$21
doi: 10.1117/12.2546734

saturation currents similar to deep p^+n-junctions[26]. It has been proposed that the formation of negative fixed charge at the PureB-Si interface increases the concentration of holes which is responsible for an effective suppression of the otherwise high electron injection into the anode[26,27]. Low saturation currents were achieved for nm-thin PureB layers deposited by CVD at temperatures from 700 °C down to 400 °C[26]. When used for UV light[26] and low-energy electrons[28] detection, diodes with PureB layers deposited at these temperatures showed high stability and robustness during high-dose and high-energy radiation/particle exposure[26].

In PureGaB Ge-on-Si technology, a wetting layer of pure gallium was introduced before the boron deposition to obtain p^+-like anode regions with low saturation currents on Ge-island photodiodes [17,29–31]. The diodes displayed ideality factors of less than 1.1 and dark current densities in the range of 15 μA/cm^2 at room temperature[30]. The devices have been demonstrated for operation as avalanche photodiodes in linear and Geiger mode[17,31]. For the latter, single-photon avalanche diodes were fabricated with a timing jitter of 900 ps FWHM and dark count rates (DCR) as low as 1 kHz at room temperature[17]. PureGaB Ge-on-Si photodiodes were fabricated in 300×1 arrays with different pixel geometries showing high reproducibility and uniformity of the electrical and optical characteristics[29,31].

In this paper, a more in depth investigation of the PureGaB Ge-on-Si photodiodes described in [29,31] will be presented. In particular, they are shown to be responsive in the spectral range from UV to NIR wavelengths. Measurements were performed using 255 nm and 280 nm light emitting diodes and 406 nm, 670 nm, 1310 nm and 1550 nm lasers. The responsivity was measured on-wafer using in-house developed optoelectronic setups. PureGaB Ge-on-Si photodiodes were also simulated with varying parameters for the pn-junction depth, Ge doping concentration, and concentration of traps at the Ge/Si interface. By comparing these simulations to the measurements, mechanisms that could lead to degradation of the responsivity in the UV and NIR wavelength ranges were identified. Light-emission from the PureGaB Ge-on-Si devices operated above breakdown voltage was measured to identify hot spots in the device. A simulation study of the breakdown characteristics was performed, and optimized PureGaB Ge-on-Si diode designs are proposed for obtaining better overall electrical and optical performance.

2. ELECTRICAL CHARACTERIZATION

2.1 Device fabrication

The PureGaB Ge-on-Si photodiodes characterized in this work were processed in two separate fabrication runs[29,31] referred in the following as *J-diodes*[29] and *T-diodes*[31]. In both runs, the starting substrates for the diode fabrication were 2-5 Ωcm n-type (100) Si wafers. The Ge-island area was defined by patterning 26×26-μm^2-large windows in a 1-μm-thick SiO_2 layer. A commercial ASM Epsilon 2000 CVD reactor was used to selectively grow Ge and deposit Ga and B, all in the same deposition run. A 50-nm-thick Ge layer was first grown at 400 °C to serve as a flat seed layer on the Si. The bulk Ge islands were then deposited at 700 °C with an arsenic n-doping of ≈ 10^{16} cm^{-3}. The final thickness of Ge islands was between 0.6 μm and 1.6 μm depending on loading effects that were controlled by patterning exposed Si region around the device structures. The dislocation density was reduced by a 1-h anneal at 750 °C which resulted in defect-densities in the order of 10^7 cm^{-2} [32]. This was followed by depositing a wetting layer of pure gallium and then capping it with a PureB layer that functions as a barrier layer between the Ge and the Al metallization. The final thickness of this PureGaB layer was approximately 25 nm[29]. Plasma-enhanced CVD (PECVD) oxide was then deposited which at the end of the process was maintained on the light entrance windows as a 1-μm-thick transparent protection layer. To contact the p-type region formed by the PureGaB, a 1-μm-wide ring along the perimeter of the Ge-on-Si photodiodes was etched through the oxide. A 900-nm-thick Al/Si(1%) was sputtered and patterned so that the central region of the PureGaB Ge islands were covered solely by oxide. The only difference in processing between the two diodes sets studied here is the metal alloying step. For *J-diodes*, alloying was performed for 30 min at 400 °C in forming gas[29], while for *T-diodes* the alloying time was extended to 1 hr[31]. The most critical step for this manner of processing was found to be the etching of the contact windows which were placed exactly within the oxide window edge. The etching was performed by first plasma etching until only a few nm of oxide was left and then completing the oxide removal by dipping in diluted HF. In some cases this exposed both the Ge-island sidewalls as well as the underlying Si to the Al metallization. In these cases an aggressive Al-mediated migration of Ge and Si was observed [29]. The Ge-on-Si photodiodes were fabricated in arrays as shown in Figure 1 having 300×1 devices in a row.

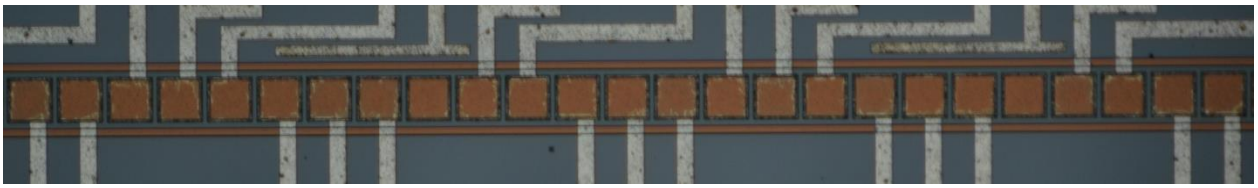

Figure 1. Optical image of 26×26 μm^2 PureGaB Ge-on-Si photodiodes that were part of an 300×1 photodiode array.

2.2 Optoelectronic measurement setups

Characterization of the fabricated devices was performed using an in-house on-wafer laser illumination setup as illustrated in Figure 2a. The system consists of a 4-channel fiber-coupled laser source from Thorlabs – MCLS1. The selected laser diodes have discrete wavelengths of λ_O = 406 nm, 670 nm, 1310 nm and 1550 nm. The power of the laser, P_O, is controlled in the range between 0.5 mW and 2 mW by a high-precision, constant-current source with a temperature control unit. The diodes-under-test were mounted in a Suss MicroTec PM300 probe station. The light beam was guided to the microscope of the probe station using a multimode fiber. Electrical characterization was performed using a Keithly 4200 parameter analyzer. Optical loses in the fiber and the focusing unit of the probe station were estimated by using Ge and Si reference photodiodes and the output power of the focused light spot on the sample, P_M, is attenuated by more than three orders of magnitude. The diameter of the focused light spot on the diode, D_M, is estimated to be smaller than 20 μm. Optical measurements were also performed using UV light-emitting diodes UVTOP255 and UVLED280TO46FW with wavelengths λ_{LED} = 255 nm and 280 nm, respectively. The output power of the UV LEDs varied between 0.2 mW and 1 mW and was controlled by the LED current, I_{LED}. In the measurement setup shown in Figure 2b, the UV LEDs were used as a blanket illumination source without measuring the output power of the diode.

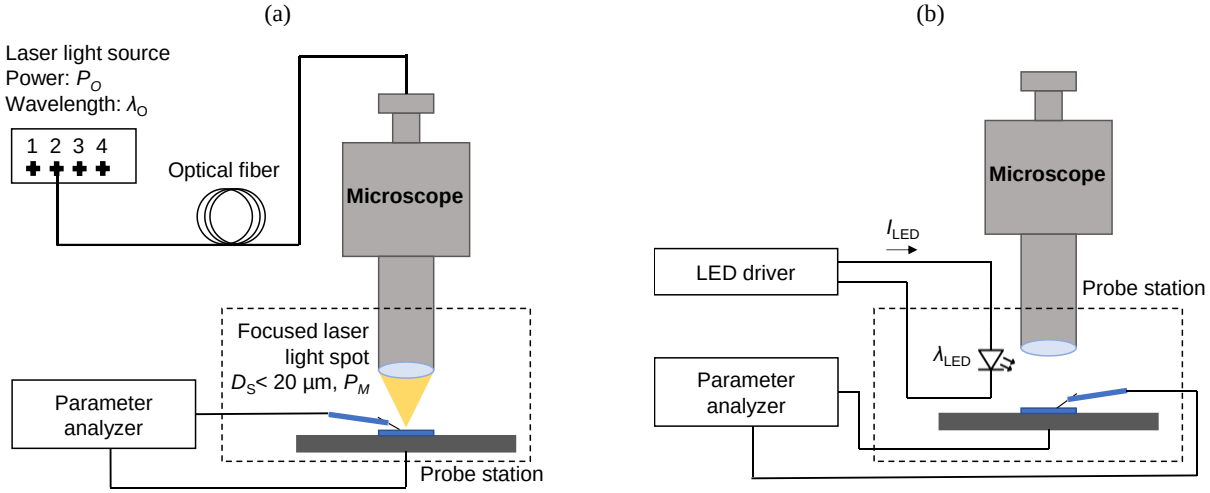

Figure 2. Schematics of the optoelectronic setups used for: (a) on-wafer responsivity measurements; (b) blanket light-illumination using ultraviolet light-emitting diodes.

2.3 Responsivity measurements

The developed measurement setups were used to determine the optical response of PureGaB Ge-on-Si photodiodes in the UV to NIR wavelength range. With the on-wafer optoelectronic measurement system, laser light was focused on a single 26×26 μm^2 photodiode. Current-voltage characteristics of a *J-diode* measured for P_O = 1 mW at the four different wavelengths are shown in Figure 3a. Photocurrents were compared to the dark current of the device and had more than two orders of magnitude higher values that remained flat irrespective of the applied reverse bias voltage. Using the LED blanket-light illumination setup, the optical response to UV light for λ_{LED} = 255 nm and I_{LED} = 10 mA, 20 mA and 30 mA, was measured, and corresponding current-voltage characteristics are shown in Figure 3b. The PureGaB Ge-on-Si photodiodes are responsive to UV light and have almost an order of magnitude higher photocurrent compared to the dark current of the device. When using λ_{LED} = 280 nm, photocurrents higher than 10 nA were measured at -2 V for I_{LED} = 30 mA. With the UV-light blanket-illumination, the light is not focused on a single PureGaB Ge-on-Si photodiode and carriers generated in Si could also contribute the total photocurrent. However, the penetration depth of UV light in the 200 nm to 300 nm wavelength range in Si is in the range of 5 nm[33], so there is a large probability for carriers generated in Si to

recombine at the Si/SiO_2 interface[34,35]. Additionally, at a reverse bias of -2 V, spreading of the depletion region is limited only to the Ge, and it is expected that carriers generated in the Ge island are the main contribution to the photocurrent.

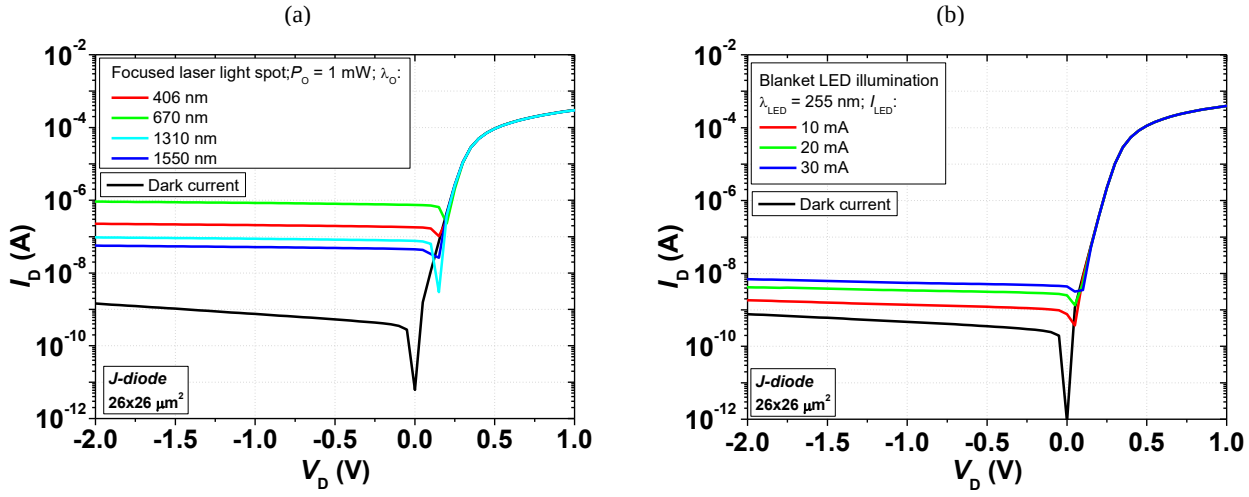

Figure 3. Current-voltage characteristics of PureGaB Ge-on-Si *J-diodes* measured using: (a) the on-wafer optoelectronic measurement setup with P_O = 1 mW at wavelengths λ_O = 406 nm, 670 nm, 1310 nm and 1550 nm; (b) blanket light-illumination setup with λ_{LED} = 255 nm.

The responsivity of four PureGaB *J-diodes* and *T-diodes* were measured at V_D = -2 V and P_O = 1 mW. The responsivity is defined as $R = I_{ph}/P_M$, where I_{ph} is the measured photocurrent. The responsivity as a function of wavelength is plotted in Figure 4a showing high device-to-device uniformity. *J-diodes* have almost an order of magnitude higher responsivity as compared to *T-diodes*. The discrepancy is attributed to a known difference in the processing of the two diode sets: in *J-diodes* the duration of Al alloying was 30 min while in *T-diodes* it was 1 hr. PureGaB Ge-on-Si photodiodes suffer from Al-mediated material transport initiated at the edges of the Ge islands if the Ge-island sidewall is left without a protective PureGaB layer to the Al metallization. During the 30 min alloy, the Al migrated up to 5 µm laterally through the Ge crystal[29], changing some of the n-Ge to p-type Al-doped Ge along the way. These bulk p-Ge regions will no longer be optically active in the NIR wavelength range. Additional alloying experiments were performed and showed conclusively that there was a detrimental effect on responsivity of the Ge-on-Si photodiodes. The responsivity as a function of laser output power at four wavelengths was also measured and is shown in Figure 4b. Small variations in responsivity for varied P_O were caused by an uncertainty in determining P_M. The responsivity remained constant irrespective of the laser power which indicates that the interface traps are filled or the depletion region did not spread into the Ge/Si interface at the given reverse bias[36].

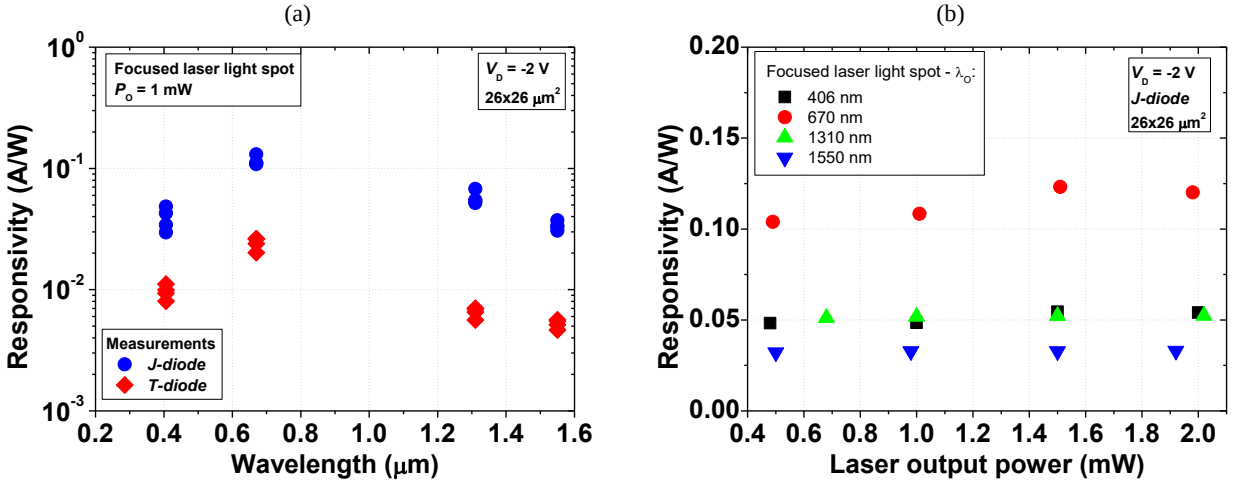

Figure 4. (a) Responsivity as a function of wavelength for four measured *J-diodes* and *T-diodes* at V_D = -2 V and P_O = 1 mW. (b) Responsivity as a function of laser output power for a *J-diode* at V_D = -2 V and λ_O = 406 nm, 670 nm, 1310 nm and 1550 nm.

2.4 Light emission measurements

In addition to the optical response, optoelectrical characterization of PureGaB Ge-on-Si photodiodes was performed by light emission measurements. Imaging of the diodes operated above the breakdown voltage, V_{BR}, can reveal hot spots in the structure, the knowledge of which can help to further improve the design[37]. The breakdown characteristics of one *J-diode* at 300 K was measured as shown in Figure 5a. The measured $V_{BR} \approx 33$ V agrees well with the values between 27 V and 35 V previously reported for *J-diodes*[29]. Light-emission measurements were performed by imaging the Ge-on-Si photodiode with a digital camera using a 20 s integration time. The diodes were biased above V_{BR}, and at V_D = -35 V light-emission spots occurred at the corners of the device as shown in Figure 5b. The light-emission spots could stem from breakdown either at the Ge sidewalls or in underlying Si. The noise characteristics of Ge-on-Si avalanche photodiodes (APDs) depend on the exact position of the breakdown and in order to minimize avalanche noise, the multiplication region is commonly placed in the Si[38]. A simulation study is performed in Section 3.2 to understand the breakdown behavior of the PureGaB Ge-on-Si photodiodes that can be expected.

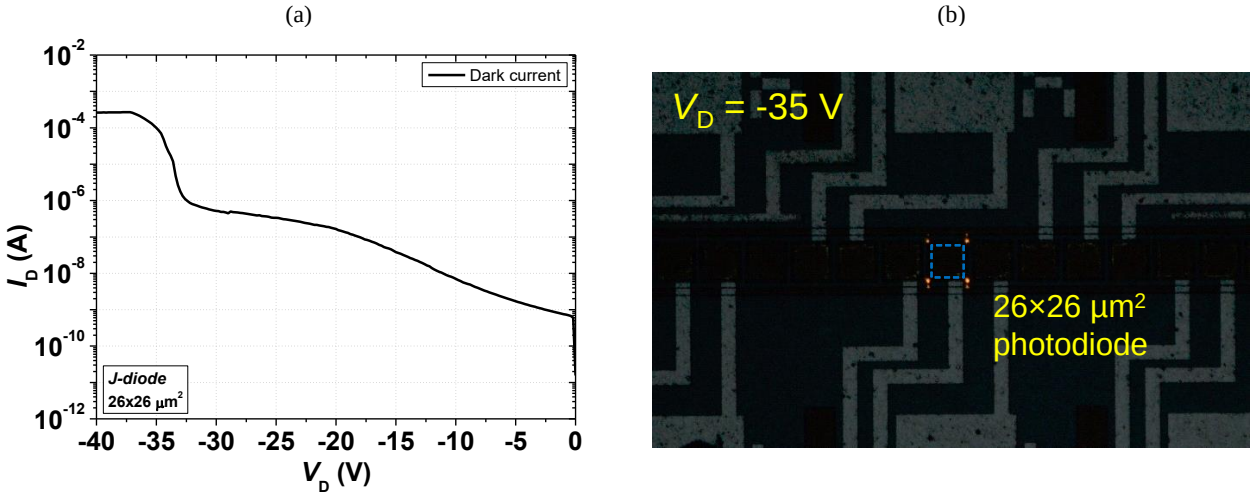

Figure 5. (a) *I-V* characteristics of a reverse biased PureGaB Ge-on-Si photodiode measured at 300 K. (b) Light-emission measurement at V_D = -35 V for the same device showing the appearance of bright spots in the corners of the device.

3. DEVICE SIMULATIONS

To further analyze the optoelectronic behavior of PureGaB Ge-on-Si photodiodes, device simulations were performed using commercially available technology-computer-aided-design (TCAD) software – Synopsys Sentaurus Device[39]. Responsivities were extracted from simulations of the Ge-on-Si structure shown in Figure 6a. The thickness of the simulated n-type Si substrate was 500 µm with a constant doping, N_{Si}, of 10^{15} cm^{-3}. The thickness of the Ge island, t_{Ge}, was varied between 0.5 µm and 1.5 µm, and the n-type doping of the Ge island, N_{Ge}, was uniform and varied from 5×10^{15} cm^{-3} to 5×10^{16} cm^{-3}. The pn junction in the Ge was formed by simulating a constant box-like p-type doping profile, $N_{p+} = 10^{20}$ cm^{-3}, and the junction depth, y_j, was varied from 5 nm to 100 nm. On top of the active Ge photodiode region, an oxide layer with thicknesses, t_{ox}, of either 0.5 or 1 µm was assumed. Carrier mobilities were modeled using the Philips unified mobility model[40] and Fermi-Dirac statistics[41] were assumed for electrons and holes. Electron and hole lifetimes of the SRH model for Si have their default values while electron and hole lifetimes of Ge, $\tau_{e,h}$, have values of 10^{-5} s, 10^{-8} s or 10^{-10} s. Optical simulations were performed using the *OptBeam* model which computes the optical generation in semiconductors by simple photon absorption using Beer's law, and the *TMM* model based on the transfer matrix approach which takes into account absorption, reflectivity and interference in simulated layers. The optical generation assumed an internal quantum yield of 1 irrespective of the wavelength. Impact ionization is simulated using the van Overstraeten-de Man[42] model.

The ideal responsivity of a Ge-on-Si photodiode is shown in Figure 6b for a simulation using the *OptBeam* model and extracted at V_D = -2 V with t_{Ge} = 1 µm, $N_{Ge} = 10^{16}$ cm^{-3}, $\tau_{e,h} = 10^{-5}$ s and y_j = 5 nm, 20 nm and 50 nm. For comparison, the simulated responsivity of similar bulk-Si and bulk-Ge photodiodes are also included. In the UV to VIS range, Ge-on-Si devices with these very shallow pn-junctions can have a responsivity which is comparable to or higher than the bulk-Si photodiodes. Responsivity in the NIR range is determined by the thickness of the Ge layer.

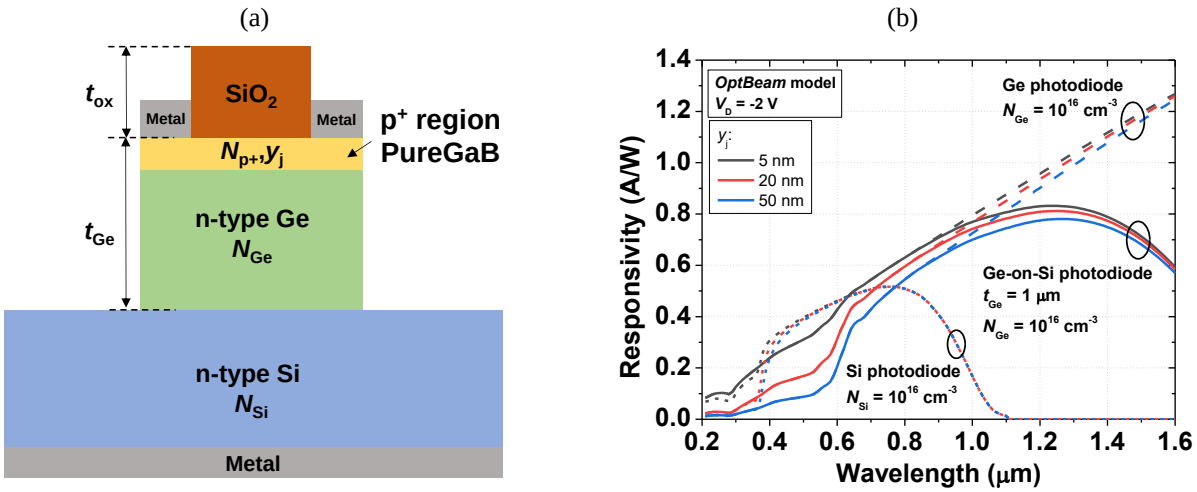

Figure 6. (a) Cross section of the simulated Ge-on-Si structure. (b) Responsivity as a function of wavelength at V_D = -2 V for Ge-on-Si structure using the *OptBeam* model with t_{Ge} = 1 µm, N_{Ge} = 10^{16} cm^{-3}, and y_j = 5 nm, 20 nm and 50 nm. Responsivities of bulk-Si and bulk-Ge photodiodes are shown for comparison.

3.1 Responsivity analysis

The measured responsivity at V_D = -2 V of *J*- and *T-diodes* is compared to the responsivity simulated using the *OptBeam* model for structures with t_{Ge} = 1 µm, N_{Ge} = 10^{16} cm^{-3}, $\tau_{e,h}$ = 10^{-5} s and y_j = 5 nm and is shown in Figure 7a. There is a large discrepancy between measurements and simulations especially for *T-diode*s which show more than two orders of magnitude lower responsivity as compared to the simulations. A simulation study is therefore performed to analyze which geometrical and physical parameters of Ge-on-Si photodiodes could have such a detrimental impact on the responsivity. In Figure 7a responsivity is also simulated for y_j set at 20 nm, 50 nm and 100 nm. The lower responsivity for 406 nm and 670 nm could be explained by a deeper junction depth which could be caused by Ga diffusion into Ge during 700 °C PureB deposition step[43,44]. However, variations in y_j were not able to explain the low measured responsivity in the NIR range. The responsivity simulated for t_{Ge} = 0.5 µm, 1 µm and 1.5 µm and $\tau_{e,h}$ = 10^{-5} s, 10^{-8} s and 10^{-10} s is shown in Figure 7b. Simulations were performed using the *OptBeam* model at V_D = -2 V and the parameters N_{Ge} = 10^{16} cm^{-3} and y_j = 5 nm. Decreasing t_{Ge} is seen to lower the responsivity in the NIR range since Ge is needed for absorption of light with wavelengths above 1.1 µm. The thickness of Ge which would give good agreement with the measurements would have to be as low as 0.1 µm. However, the Ge-on-Si thickness determined from TEM analysis shows values between 0.6 µm and 1.6 µm[29]. Decreasing hole and electron lifetime also decreases responsivity, but only for lifetimes shorter than 10^{-10} s. Changing the doping concentration to values N_{Ge} = 5×10^{15} cm^{-3}, 10^{16} cm^{-3} and 5×10^{16} cm^{-3} did not impact the responsivity at all.

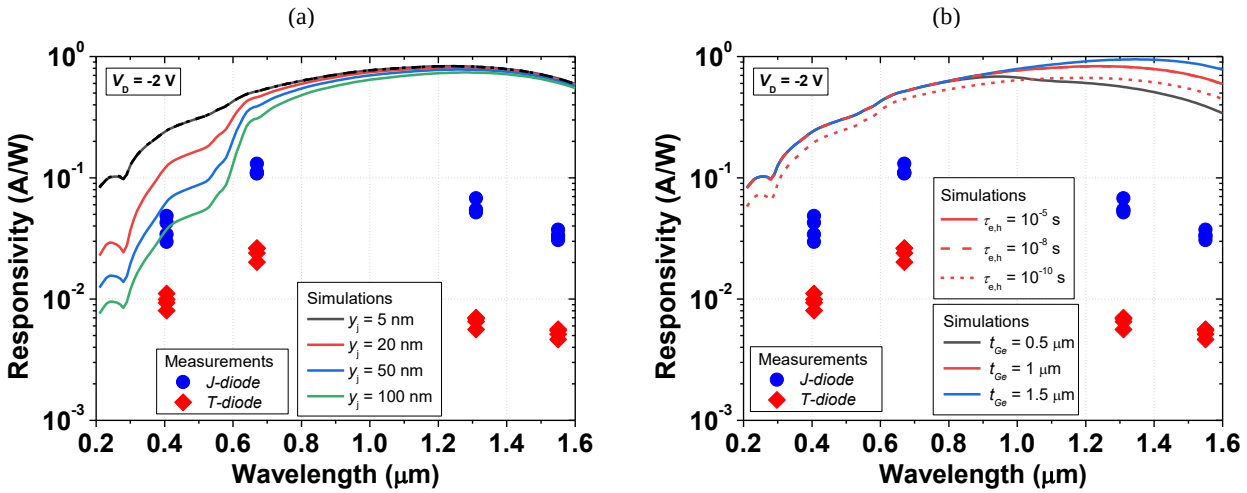

Figure 7. Simulated responsivity using the *OptBeam* optical generation model at V_D = -2 V as a function of wavelength compared to the measured responsivity of *J*- and *T-diodes* for: (a) y_j = 5 nm, 20 nm, 50 nm and 100 nm, t_{Ge} = 1 µm, N_{Ge} = 10^{16} cm^{-3}, $\tau_{e,h}$ = 10^{-5} s; (b) t_{Ge} = 0.5 µm, 1 µm and 1.5 µm and $\tau_{e,h}$ = 10^{-5} s, 10^{-8} s and 10^{-10} s, N_{Ge} = 10^{16} cm^{-3} and y_j = 5 nm.

The impact of reflectivity and interference of the oxide layer is analyzed by performing simulations using the *TMM* model. The responsivity as a function of wavelength is shown in Figure 8 for structure with t_{ox} = 0.5 µm and 1 µm and compared to simulations using only the *OptBeam* model. Since oxide is transparent in the simulated range of wavelengths, the *OptBeam* model gave the same responsivity irrespective of the oxide thickness. The simulated responsivity using the *TMM* model shows that the impact of reflectivity and interference is not able to explain the significant drop in responsivity in the UV and NIR range.

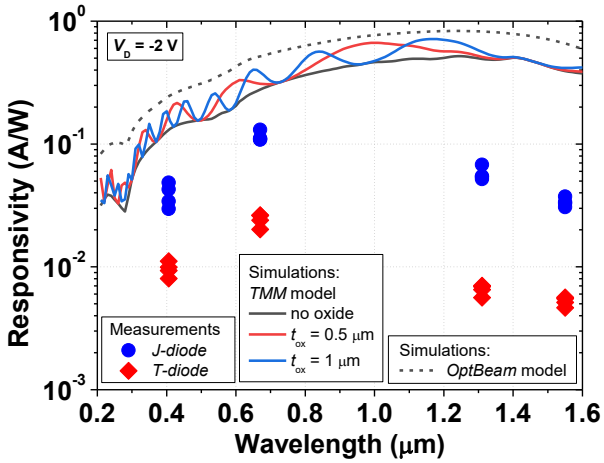

Figure 8. Simulated responsivity using the *TMM* optical generation model at V_D = -2 V as a function of wavelength compared to the measured responsivity of *J*- and *T-diodes* for y_j = 5 nm, t_{Ge} = 1 µm, N_{Ge} = 10^{16} cm^{-3}, $\tau_{e,h}$ = 10^{-5} s and t_{ox} = 0.5 µm and 1 µm. Simulated responsivity using the *OptBeam* optical generation model is shown for comparison.

The heterojunction between Ge and Si is also considered as a possible source of deteriorated PureGaB Ge-on-Si photodiode responsivity. The Ge/Si interface traps are known to impact both the static and dynamic performance of photodiodes[36,45,46]. Both donor and acceptor traps are found to be located in the lower part of Ge bandgap close to the valence band[45,46]. Charged acceptor states are found at energies of E_{acc}=E_v + 0.11 eV while charged donor states are located at E_{don}=E_v + 0.05 eV, where E_v is the valence band edge[45,46]. The Ge/Si interface traps tend to be p-type irrespective of the bulk conductivity[36,46]. To test the impact of Ge/Si interface traps on responsivity of the PureGaB Ge-on-Si photodiodes, simulations were performed assuming trap concentration at the Ge/Si interface, N_T, varied from 10^{10} to 10^{14} cm^{-2}. The simulated capture cross section for electrons and holes was σ_T = 10^{-13} cm^2 [45]. The impact of both trap types on responsivity was simulated individually, and the results for acceptors and donors are shown in Figure 9a and 9b, respectively. The trap energy for acceptors was E_{acc} = E_{Fi} - 0.25 eV while the trap energy for donors was E_{don}= E_{Fi} - 0.3 eV, where E_{Fi} is the intrinsic Fermi level. Optical simulations were performed using the *TMM* model with t_{ox} = 1 µm while other parameters were y_j = 5 nm, t_{Ge} = 0.5 µm, N_{Ge} = 10^{16} cm^{-3}, $\tau_{e,h}$ = 10^{-5} s. Results are shown for N_T varied from 10^{10} cm^{-2} to 7×10^{13} cm^{-2}. The simulated responsivity of PureGaB Ge-on-Si photodiodes with Ge/Si acceptor interface traps, as shown in Figure 9a, indicates that the higher trap concentrations could explain the measured decrease in responsivity observed in the whole UV to NIR range. For *J-diodes*, the concentration of interface traps which fits the measured values is 2×10^{13} cm^{-2} while for *T-diodes* this concentration increases to 7×10^{13} cm^{-2}. In both cases, the simulated responsivity gives a good approximation of the measurements from the UV to NIR wavelength range indicating that a higher concentration of acceptor traps could indeed explain the lower responsivity. It is expected that the traps do not uniformly occupy the whole interface but are mainly located close to edges that are known to be affected by Al-mediated material transport[29]. This is consistent with measurements performed on *T-diodes* which were subject to a longer thermal step during Al alloying and display lower responsivity. As shown in Figure 9b, donor traps do not impact responsivity irrespective of the concentration.

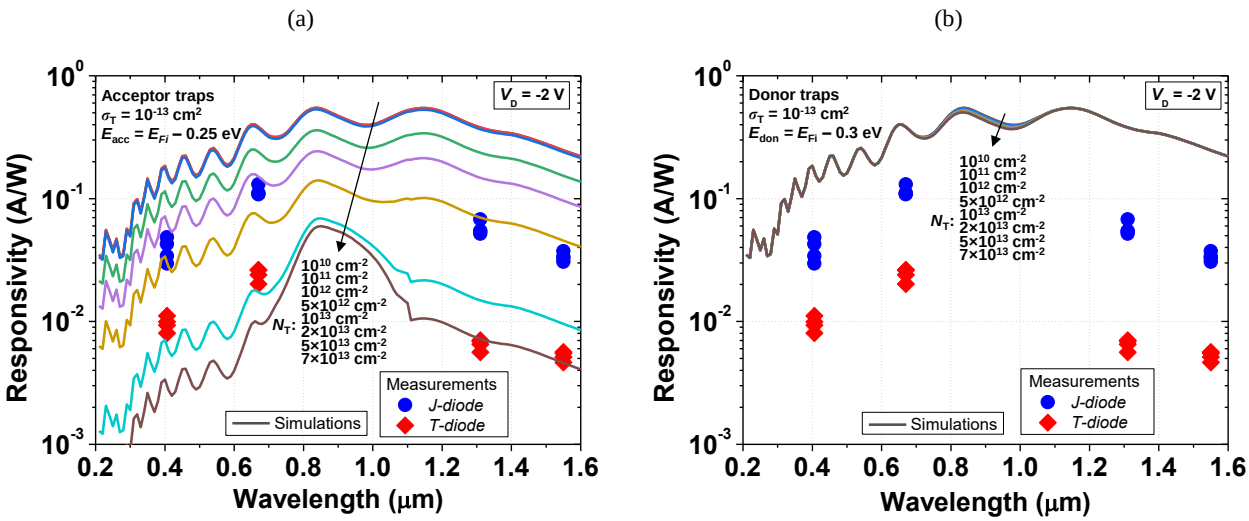

Figure 9. Simulated responsivity using the *TMM* optical generation model at V_D = -2 V, as a function of wavelength and compared to the measured responsivity of *J*- and *T-diodes* for an N_T of: (a) acceptor traps with σ_T = 10^{-13} cm^2, E_{acc} = E_{Fi} – 0.25 eV; (b) donor traps with σ_T = 10^{-13} cm^2, E_{don} = E_{Fi} – 0.3 eV. The other parameters used in the simulations were y_j = 5 nm, t_{Ge} = 0.5 μm, N_{Ge} = 10^{16} cm^{-3}, $\tau_{e,h}$ = 10^{-5} s, t_{ox} = 1 μm.

3.2 PureGaB Ge-on-Si photodiode geometry optimization

In order to minimize the impact of Al migration from the Ge sidewalls, the contacts to the Ge island should preferably be processed to only contact the PureGaB layer. Contacting to the Ge sidewalls is an advantage for the fill factor but the process should then be modified to expose the sidewalls to a complete PureGaB coverage before metal deposition. The B layer has high resistivity so to maintain low series resistance, layers thinner than the tunneling thickness of about 3 nm should be applied. The effective barrier and resistance properties of 2-nm-thick B layers have already been demonstrated in PureB Si photodiodes[47]. A simulation analysis was performed to investigate the electrical performance of such a photodetector with complete PureGaB-all-round coverage of the Ge island surface. Electrical simulations were performed with the device structure illustrated in Figure 10. In-diffusion of Ga and/or B from the PureGaB-all-around electrode was set to have vertical (y_j) and lateral (x_j) pn-junctions with x_j = y_j = 5 nm, 10 nm, 50 nm and 100 nm. Other parameters used in the simulations were N_{Ge} = 10^{16} cm^{-3}, t_{Ge} = 1 μm, $\tau_{e,h}$ = 10^{-5} s. The thickness of the simulated n-type bulk Si was 500 μm with a constant doping, N_{Si}, of 10^{15} cm^{-3}. Even with a very deep vertical and lateral pn-junction of 100 nm the total responsivity of a 26×26 μm^2 PureGaB-all-around diode would decrease less than 1 % compared to structure with only a top-surface PureGaB region. The impact of a shallower pn-junction on the responsivity would be even less significant. Breakdown simulations were performed to check the impact of lateral pn-junction on V_{BR}.

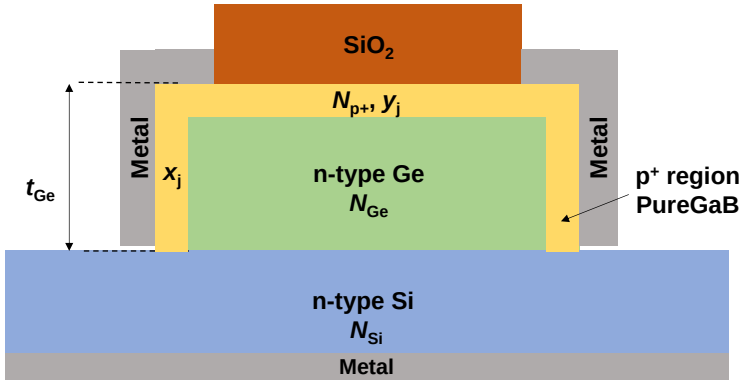

Figure 10. Cross section of the PureGaB-all-around Ge-on-Si photodiode structure.

The simulations of the PureGaB Ge-on-Si photodiodes with only a top-surface PureGaB layer, as shown in Figure 6a, were performed first and compared to the experimental breakdown voltage and light-emission analysis performed in Section 2.4. The *I-V* characteristics found from the breakdown simulations are shown in Figure 11a. The simulated 2D impact ionization generation rate at $V_D = -V_{BR}$ is shown in Figure 11b. The simulated breakdown voltage is 32 V which matches well with measured values, and the position of the maximum impact ionization matches the light-emission measurements of Figure 5b that showed breakdown at the corners of the device. The maximum impact ionization is located at the Ge island sidewall.

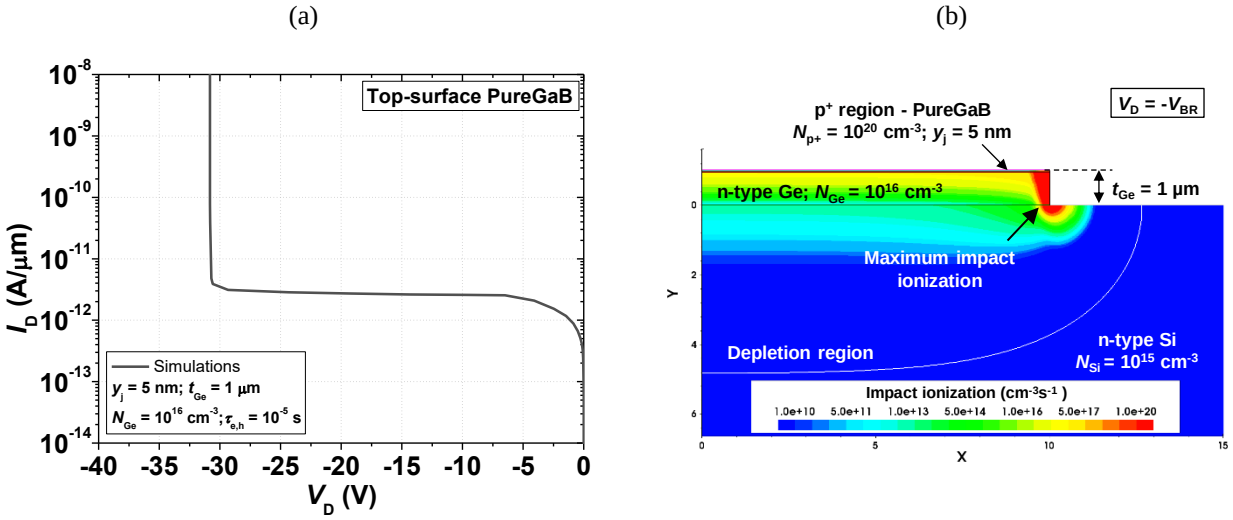

Figure 11. (a) Simulated breakdown characteristics of a PureGaB Ge-on-Si photodiode with a top-surface PureGaB layer. (b) Impact ionization generation rate at $V_D = -V_{BR}$.

The breakdown voltages in the PureGaB-all-around design were simulated for varied $x_j = y_j$ = 5 nm, 10 nm, 50 nm, 100 nm and the results are shown in Figure 12a. The *I-V* characteristics display a decrease of the breakdown voltage as the junction becomes shallower. The main reason for this is the electric field distribution in Si under the PureGaB-all-around electrode which causes an increase of impact ionization generation rate as shown in Figure 12b for the PureGaB-all-around structure with $x_j = y_j$ = 50 nm at $V_D = -V_{BR}$.

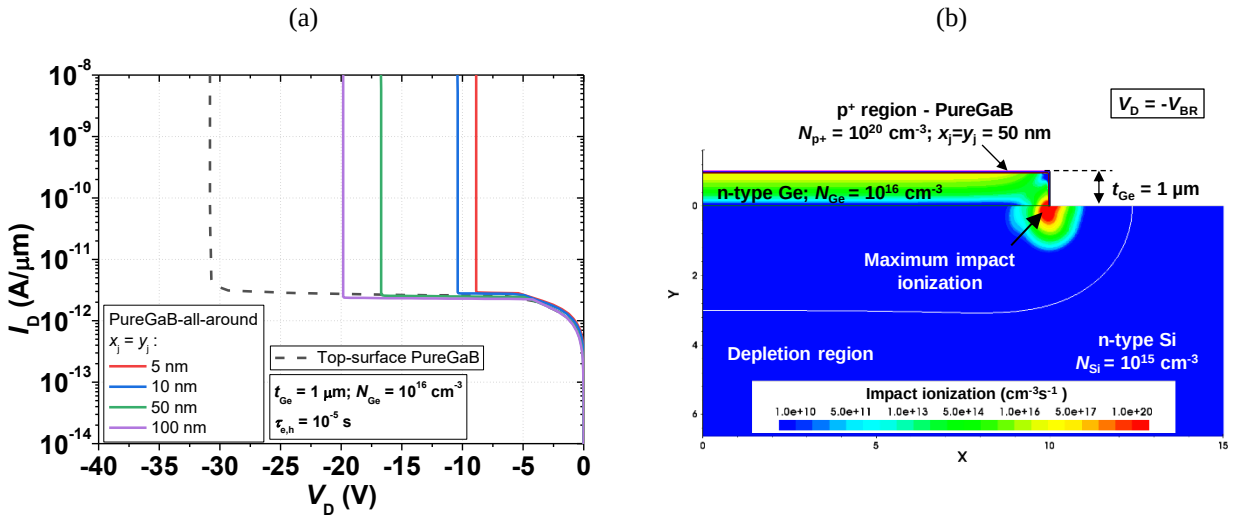

Figure 12. (a) Simulated breakdown characteristics of PureGaB-all-around Ge-on-Si photodiodes with $x_j = y_j$ = 5 nm, 10 nm, 50 nm and 100 nm. Simulations of the top-surface contacted PureGaB Ge-on-Si photodiode are shown for comparison. (b) Impact ionization generation rate of the PureGaB-all-around Ge-on-Si photodiode with $x_j = y_j$ = 50 nm at $V_D = -V_{BR}$.

In order to prevent premature breakdown for extremely shallow pn-junctions in case of the PureGaB-all-around Ge-on-Si photodiode, a guard ring (GR) is added in the Si under the Ge island. The cross section of the structure with two GRs is given in Figure 13a. Breakdown simulations were performed with GRs which had a Gaussian doping profile with junction depth of 0.5 µm, a maximum doping concentration of 10^{18} cm^{-3} and lateral spreading, L_{GR}, of 0.5 µm. Results are shown in Figure 13b for $x_j = y_j$ = 5 nm, 10 nm, 50 nm, 100 nm. In all cases, the breakdown voltage increases to values higher than 55 V.

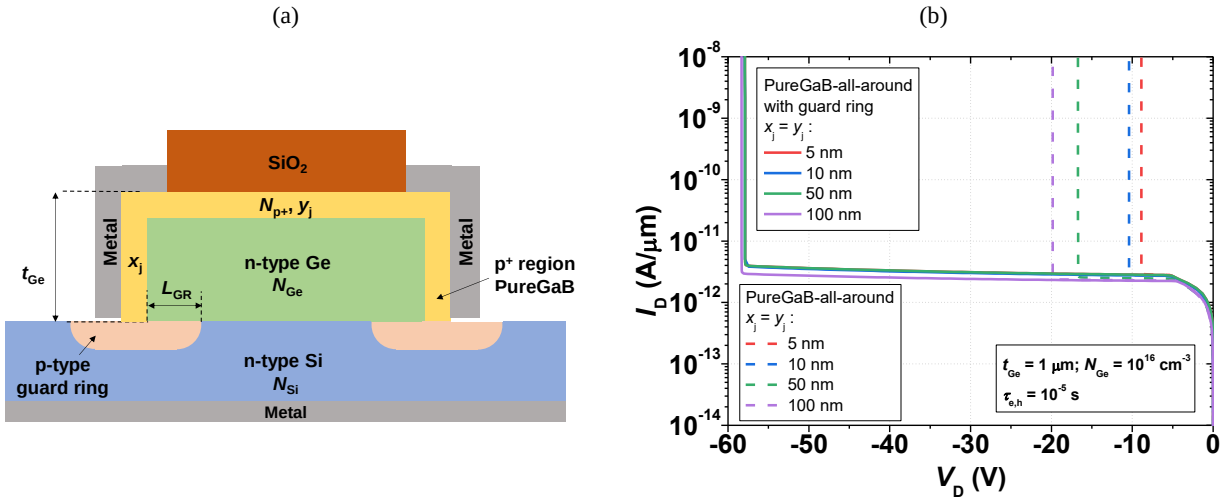

Figure 13. (a) Cross section of a PureGaB-all-around Ge-on-Si photodiode with p-type guard rings. (b) Simulated breakdown characteristics of a PureGaB-all-around Ge-on-Si photodiode with and without guard rings.

4. CONCLUSIONS

Optical characterization of PureGaB Ge-on-Si photodiodes showed that the devices were responsive in the whole UV to NIR range. Photocurrents as high as 10 nA were measured by illuminating PureGaB photodiodes with bulk UV light sources with wavelengths of 255 nm and 280 nm. The responsivity was determined at discrete wavelengths of 406 nm, 670 nm, 1310 nm and 1550 nm for two sets of devices. The one set displayed up to a decade lower responsivity than would be expected on the basis of the simulations, while the other had values yet another decade lower. This degradation of the responsivity was found to be related to Al-mediated material transport during the metal alloying step, initiated at the perimeter of the Ge islands if they were not covered with a PureGaB layer. A simulation study performed on different Ge-on-Si structures showed that the presence of acceptor traps at Ge/Si interface could explain the decrease of responsivity in the whole UV to NIR range. These acceptor states could in reality be Al-dopants activated during the Al-mediated material transport. While the electrical properties of the PureGaB devices were not degraded, the results underline that having a barrier such as the B-layer between the Ge/Si and the metal is of importance for maintaining the optical performance.

A modification of the basic diode structure was proposed where the PureGaB layer was deposited around the whole Ge island surface. The electrical and optical properties of this PureGaB-all-around structure were studied via simulations. Due to the extremely shallow nature of the PureGaB junctions, the responsivity only marginally degraded. Electrical simulations revealed that the breakdown voltage would be significantly reduced in such a geometry, going from about 35 V to as low as 8 V, and the maximum impact ionization would be located in the Si where it meets the PureGaB layer. The addition of p-type guard rings at the device perimeter was found to be a way of mitigating premature breakdown and V_{BR} could be increased to values higher than 55 V. Such a high breakdown voltage could facilitate fabrication of broadband APDs with separate charge absorption and multiplication layers in Ge-on-Si technology further increasing the sensitivity of the photodiodes.

ACKNOWLEDGEMENT

The authors would like to thank A. Sammak for the device fabrication. This work was supported by the Croatian Science Foundation under the project IP-2018-01-5296 and Unity Through Knowledge Fund (UKF) - agreement number 20/19.

REFERENCES

[1] Zhang, J., Itzler, M. A., Zbinden, H. and Pan, J.-W., "Advances in InGaAs/InP single-photon detector systems for quantum communication," Light: Science & Applications **4**(5), e286 (2015).

[2] Razeghi, M. and Rogalski, A., "Semiconductor ultraviolet detectors," Journal of Applied Physics **79**(10), 7433–7473 (1996).

[3] Takai, I., Matsubara, H., Soga, M., Ohta, M., Ogawa, M. and Yamashita, T., "Single-Photon Avalanche Diode with Enhanced NIR-Sensitivity for Automotive LIDAR Systems," Sensors **16**(4), 459 (2016).

[4] Veis, P., Marín-Roldán, A. and Krištof, J., "Simultaneous vacuum UV and broadband UV–NIR plasma spectroscopy to improve the LIBS analysis of light elements," Plasma Sources Sci. Technol. **27**(9), 095001 (2018).

[5] Sadate-Moualeua, S., Brantley, C. L., Farley, C., Kassu, A., Mills, J., Edwards, E., Ruffin, P. and Sharma, A., "Broadband optical sensing/detection technology for missile systems," Novel Optical Systems Design and Optimization XXI, C. F. Hahlweg and J. R. Mulley, Eds., 8, SPIE, San Diego, United States (2018).

[6] Skippon, S. M. and Short, R. T., "Suitability of flame detectors for offshore applications," Fire Safety Journal **21**(1), 1–10 (1993).

[7] Gong, X., Tong, M., Xia, Y., Cai, W., Moon, J. S., Cao, Y., Yu, G., Shieh, C.-L., Nilsson, B. and Heeger, A. J., "High-Detectivity Polymer Photodetectors with Spectral Response from 300 nm to 1450 nm," Science **325**(5948), 1665–1667 (2009).

[8] Yang, F., Cong, H., Yu, K., Zhou, L., Wang, N., Liu, Z., Li, C., Wang, Q. and Cheng, B., "Ultrathin Broadband Germanium–Graphene Hybrid Photodetector with High Performance," ACS Appl. Mater. Interfaces **9**(15), 13422–13429 (2017).

[9] Sood, A. K., Zeller, J. W., Ghuman, P., Babu, S. R., Dhar, N. K., Ganguly, S., Ghosh, A. W. and Dupuis, R. D., "Development of high-performance detector technology for UV and IR applications," Sensors, Systems, and Next-Generation Satellites XXIII, S. P. Neeck, T. Kimura, and P. Martimort, Eds., 39, SPIE, Strasbourg, France (2019).

[10] Huang, Z., Jiang, Y., Han, Q., Yang, M., Han, J., Wang, F., Luo, M., Li, Q., Zhu, H., Liu, X., Gou, J. and Wang, J., "High responsivity and fast UV–vis–short-wavelength IR photodetector based on Cd_3As_2/MoS_2 heterojunction," Nanotechnology **31**(6), 064001 (2020).

[11] Yang, W., Hu, K., Teng, F., Weng, J., Zhang, Y. and Fang, X., "High-Performance Silicon-Compatible Large-Area UV-to-Visible Broadband Photodetector Based on Integrated Lattice-Matched Type II Se/n-Si Heterojunctions," Nano Lett. **18**(8), 4697–4703 (2018).

[12] Hosseini, Z. S., Bafrani, H. A., Naseri, A. and Moshfegh, A. Z., "High-performance UV-Vis-NIR photodetectors based on plasmonic effect in Au nanoparticles/ZnO nanofibers," Applied Surface Science **483**, 1110–1117 (2019).

[13] Goossens, S., Navickaite, G., Monasterio, C., Gupta, S., Piqueras, J. J., Pérez, R., Burwell, G., Nikitskiy, I., Lasanta, T., Galán, T., Puma, E., Centeno, A., Pesquera, A., Zurutuza, A., Konstantatos, G. and Koppens, F., "Broadband image sensor array based on graphene–CMOS integration," Nature Photon **11**(6), 366–371 (2017).

[14] Jiang, J., Chu, J. H. and Banerjee, K., "CMOS-Compatible Doped-Multilayer-Graphene Interconnects for Next-Generation VLSI," 2018 IEEE International Electron Devices Meeting (IEDM), 34.5.1-34.5.4, IEEE, San Francisco, CA (2018).

[15] Michel, J., Liu, J. and Kimerling, L. C., "High-performance Ge-on-Si photodetectors," Nature Photonics **4**(8), 527–534 (2010).

[16] Liu, J., Camacho-Aguilera, R., Bessette, J. T., Sun, X., Wang, X., Cai, Y., Kimerling, L. C. and Michel, J., "Ge-on-Si optoelectronics," Thin Solid Films **520**(8), 3354–3360 (2012).

[17] Sammak, A., Aminian, M., Qi, L., de Boer, W. B., Charbon, E. and Nanver, L. K., "A CMOS compatible Ge-on-Si APD operating in proportional and Geiger modes at infrared wavelengths," Electron Devices Meeting (IEDM), 2011 IEEE International, 8–5, IEEE (2011).

[18] Aspnes, D. E. and Studna, A. A., "Dielectric functions and optical parameters of Si, Ge, GaP, GaAs, GaSb, InP, InAs, and InSb from 1.5 to 6.0 eV," Phys. Rev. B **27**(2), 985–1009 (1983).

[19] Wilkinson, F. J., Farmer, A. J. D. and Geist, J., "The near ultraviolet quantum yield of silicon," Journal of Applied Physics **54**(2), 1172–1174 (1983).

[20] Antoncik, E. and Gaur, N. K. S., "Theory of the quantum efficiency in silicon and germanium," J. Phys. C: Solid State Phys. **11**(4), 735–744 (1978).

[21] Satta, A., Simoen, E., Janssens, T., Clarysse, T., De Jaeger, B., Benedetti, A., Hoflijk, I., Brijs, B., Meuris, M. and Vandervorst, W., "Shallow Junction Ion Implantation in Ge and Associated Defect Control," Journal of The Electrochemical Society **153**(3), G229 (2006).
[22] Chuang, S.-S., Cho, T.-C., Sung, P.-J., Kao, K.-H., Chen, H. J. H., Lee, Y.-J., Current, M. I. and Tseng, T.-Y., "Ultra-Shallow Junction Formation by Monolayer Doping Process in Single Crystalline Si and Ge for Future CMOS Devices," ECS J. Solid State Sci. Technol. **6**(5), P350–P355 (2017).
[23] Li, J., Cheng, R., Liu, C., Zhang, P., Lu, J., Chen, K., Zhang, R. and Zhao, Y., "High performance Ge ultra-shallow junctions fabricated by a novel formation technique featuring spin-on dopant and laser annealing for sub-10nm technology applications," Microelectronic Engineering **168**, 1–4 (2017).
[24] Sharp, J., Lee, W. J., Ploog, K., Umana-Membreno, G. A., Faraone, L. and Dell, J. M., "A novel technique for degenerate p-type doping of germanium," Solid-State Electronics **89**, 146–152 (2013).
[25] Warburton, R. E., Intermite, G., Myronov, M., Allred, P., Leadley, D. R., Gallacher, K., Paul, D. J., Pilgrim, N. J., Lever, L. J. M., Ikonic, Z., Kelsall, R. W., Huante-Ceron, E., Knights, A. P. and Buller, G. S., "Ge-on-Si Single-Photon Avalanche Diode Detectors: Design, Modeling, Fabrication, and Characterization at Wavelengths 1310 and 1550 nm," IEEE Trans. Electron Devices **60**(11), 3807–3813 (2013).
[26] Nanver, L. K., Qi, L., Mohammadi, V., Mok, K. R. M., de Boer, W. B., Golshani, N., Sammak, A., Scholtes, T. L. M., Gottwald, A., Kroth, U. and Scholze, F., "Robust UV/VUV/EUV PureB Photodiode Detector Technology With High CMOS Compatibility," IEEE Journal of Selected Topics in Quantum Electronics **20**(6), 306–316 (2014).
[27] Knezevic, T., Liu, X., Hardeveld, E., Suligoj, T. and Nanver, L. K., "Limits on Thinning of Boron Layers With/Without Metal Contacting in PureB Si (Photo)Diodes," IEEE Electron Device Lett. **40**(6), 858–861 (2019).
[28] Šakić, A., Nanver, L. K., Veen, G. van, Kooijman, K., Vogelsang, P., Scholtes, T. L. M., Boer, W. de, Wien, W. H. A., Milosavljević, S., Heerkens, C. T. H., Knežević, T. and Spee, I., "Versatile silicon photodiode detector technology for scanning electron microscopy with high-efficiency sub-5 keV electron detection," 2010 International Electron Devices Meeting, 31.4.1-31.4.4 (2010).
[29] Sammak, A., Qi, L. and Nanver, L. K., "Restricted-Access Al-Mediated Material Transport in Al Contacting of PureGaB Ge-on-Si p+n Diodes," Journal of Electronic Materials **44**(12), 4676–4683 (2015).
[30] Sammak, A., Aminian, M., Qi, L., de Boer, W. B., Charbon, E. and Nanver, L. K., "Fabrication of Pure-GaB Ge-on-Si Photodiodes for Well-Controlled 100-pA-Level Dark Currents," ECS Transactions **64**(6), 737–745 (2014).
[31] Sammak, A., Aminian, M., Nanver, L. K. and Charbon, E., "CMOS-Compatible PureGaB Ge-on-Si APD Pixel Arrays," IEEE Transactions on Electron Devices **63**(1), 92–99 (2016).
[32] Sammak, A., de Boer, W. and Nanver, L. K., "Ge-on-Si: Single-Crystal Selective Epitaxial Growth in a CVD Reactor," ECS Transactions **50**(9), 507–512 (2013).
[33] Scholze, F., Henneken, H., Kuschnerus, P., Rabus, H., Richter, M. and Ulm, G., "Determination of the electron–hole pair creation energy for semiconductors from the spectral responsivity of photodiodes," Nuclear Instruments and Methods in Physics Research Section A: Accelerators, Spectrometers, Detectors and Associated Equipment **439**(2–3), 208–215 (2000).
[34] Canfield, L. R., Kerner, J. and Korde, R., "Stability and quantum efficiency performance of silicon photodiode detectors in the far ultraviolet," Applied Optics **28**(18), 3940–3943 (1989).
[35] Ouchi, H., Mukai, T., Kamei, T. and Okamura, M., "Silicon pn junction photodiodes sensitive to ultraviolet radiation," IEEE Transactions on Electron Devices **26**(12), 1965–1969 (1979).
[36] Gity, F., Daly, A., Snyder, B., Peters, F. H., Hayes, J., Colinge, C., Morrison, A. P. and Corbett, B., "Ge/Si heterojunction photodiodes fabricated by low temperature wafer bonding," Optics Express **21**(14), 17309 (2013).
[37] Krakers, M., Knezevic, T. and Nanver, L. K., "Reverse breakdown and light-emission patterns studied in Si PureB SPADs," 2019 42nd International Convention on Information and Communication Technology, Electronics and Microelectronics (MIPRO), 30–35, IEEE, Opatija, Croatia (2019).
[38] Kang, Y., Zadka, M., Litski, S., Sarid, G., Morse, M., Paniccia, M. J., Kuo, Y.-H., Bowers, J., Beling, A., Liu, H.-D., McIntosh, D. C., Campbell, J. and Pauchard, A., "Epitaxially-grown Ge/Si avalanche photodiodes for 1.3 μm light detection," Optics Express **16**(13), 9365 (2008).
[39] Synopsys., [Sentaurus Device User Guide Version N-2017.09], Synopsys, Mountain View, CA, USA (2017).
[40] Klaassen, D. B. M., "A unified mobility model for device simulation—I. Model equations and concentration dependence," Solid-State Electronics **35**(7), 953–959 (1992).

[41] Sze, S. M. and Ng, K. K., [Physics of Semiconductor Devices, 3rd edition], Wiley-Interscience, Hoboken, N.J (2006).
[42] Van Overstraeten, R. and De Man, H., "Measurement of the ionization rates in diffused silicon p-n junctions," Solid-State Electronics **13**(5), 583–608 (1970).
[43] Impellizzeri, G., Mirabella, S., Irrera, A., Grimaldi, M. G. and Napolitani, E., "Ga-implantation in Ge: Electrical activation and clustering," Journal of Applied Physics **106**(1), 013518 (2009).
[44] Petrovna, K. S., Anfimov, I. and Yurchuk, S., "Phosphorus and Gallium Diffusion in Ge Sublayer of In0.01Ga0.99As/In0.56Ga0.44P/Ge Heterostructures," [Advanced Material and Device Applications with Germanium], S. Lee, Ed., InTech (2018).
[45] Gity, F., Hayes, J. M., Corbett, B. and Morrison, A. P., "Modeling the Effects of Interface Traps on the Static and Dynamic Characteristics of Ge/Si Avalanche Photodiodes," IEEE Journal of Quantum Electronics **47**(6), 849–857 (2011).
[46] Tsipas, P. and Dimoulas, A., "Modeling of negatively charged states at the Ge surface and interfaces," Appl. Phys. Lett. **94**(1), 012114 (2009).
[47] Šakić, A., Jovanović, V., Maleki, P., Scholtes, T. L., Milosavljević, S. and Nanver, L. K., "Characterization of amorphous boron layers as diffusion barrier for pure aluminium," MIPRO, 2010 Proceedings of the 33rd International Convention, 26–29, IEEE (2010).